Influence of Ionic Complexes on Phase Behavior of Polystyrene-*b*-poly(methyl methacrylate) Copolymers

Jia-Yu Wang,† Wei Chen,† Cecile Roy,‡ James D. Sievert,† and Thomas P. Russell*,†

Department of Polymer Science and Engineering, University of Massachusetts, Amherst, Massachusetts 01003, and Unite de chimie et physique des hauts polymers, Université Catholique de Louvain-La-Neuve, Louvain La Neuve 1348, Belgium

Received August 22, 2007; Revised Manuscript Received November 15, 2007

ABSTRACT: The influence of ionic complexes on phase behavior of PS-*b*-PMMA copolymers over a wide range of molecular weights and PS volume fractions was investigated by small-angle X-ray scattering (SAXS), grazing incidence small-angle X-ray scattering (GISAXS), transmission electron microscopy (TEM), and neutron reflectivity (NR). The disorder-to-order transition (DOT) in both symmetric and asymmetric copolymers indicates that the overall Flory−Huggins segmental interaction parameter, χ_{eff}, between polystyrene (PS) and poly(methyl methacrylate) (PMMA) blocks with lithium−PMMA complexes is increased compared to that of the neat copolymers. This enhanced χ_{eff} further results in an order-to-order transition (OOT), from spheres to cylinders, and an increase in the ordering and spacing of microdomains. Moreover, transitional metal ionic complexes, such as copper−PMMA complexes, are found to have the similar influence on phase behavior of PS-*b*-PMMA copolymers. The formation of ionic complexes in the copolymers not only offers a parameter to tune the degree of microphase separation of PS-*b*-PMMA copolymers but also provides a way to fabricate multifunctional materials.

Introduction

Diblock copolymers, comprising two chemically dissimilar polymer chains that are covalently bonded together at one end, self-assemble into morphologies consisting of arrays of microdomains that are tens of nanometers in size, making them ideal for the fabrication of high-density templates for use in data storage and microelectronic devices.[1−4] The phase behavior of diblock copolymers is controlled by the volume fraction of one component *f* and the degree of microphase separation χN, where *N* is the degree of polymerization and χ is the Flory−Huggins segmental interaction parameter. At low χN, diblock copolymers are phase-mixed. As χN increases, a disorder-to-order transition (DOT) occurs. In the ordered state, diblock copolymers can form arrays of nanoscopic spherical, cylindrical, gyroid, and lamella microdomains by varying *f*. The size of the microdomains (<100 nm) is dictated by the total molecular weight of the copolymer.[5,6] The minimum size of the microdomains achievable is dictated by χ since the larger χ is, the smaller *N* can be before the copolymer phase mixes. With decreasing domain size, the average center-to-center distance between the microdomains decreases and, as such, the areal density increases.[7]

Polystyrene-*b*-poly(methyl methacrylate) (PS-*b*-PMMA) copolymers have been investigated in numerous laboratories for the generation of nanoporous templates in thin films through the control of the orientation of the microdomains by manipulating surface interactions[8] or by use of an external electric field.[9] However, because of the weak segmental interaction ($\chi = 0.038$ at 170 °C[10]), obtaining films that show a long-range lateral order or templates with smaller pore sizes less than 10 nm has been a challenge.[11] Moreover, because of the weak temperature dependence of χ ($\chi = (0.028 \pm 0.002) + (3.9 \pm 0.06)/T$)),[10] the degree of microphase separation can only be realistically tuned by changing the degree of polymerization *N*, which is rather tedious. In addition, if *N* is too large, the kinetics is slow and the viscosity is high, both of which will hamper the processing and use of the copolymers.[11] Recently, we found an increase of microdomain spacing and degree of ordering in a symmetric PS-*b*-PMMA copolymer as a consequence of the formation of lithium−PMMA complexes via the coordination of lithium ions with carbonyl groups in PMMA.[12,13] In addition, a transition in kinetic pathway of the orientation of lamellar microdomains in thin films under an applied electric field was observed from microdomain disruption and re-formation to grain rotation, which can only occur in strong segregation regime. On the basis of these observations, we proposed that the segmental interaction parameter χ between PS and PMMA increased as lithium−PMMA complexes formed.

The influence of metal ions on phase behavior of block copolymers containing poly(ethylene oxide) (PEO) or poly(vinylpyridine) (PVP) block, which can strongly coordinate with metal ions, has been reported. Mayes and co-workers observed a significant increase in the order-to-disorder transition temperature (ODT) in poly(methyl methacrylate)-*b*-poly(oligooxyethylene methacrylate) (PMMA-*b*-POEM) copolymers with lithium trifluoromethanesulfonate ($LiCF_3SO_3$) complexing the PEO side chains.[14] Bates and co-workers investigated the influence of lithium perchlorate ($LiClO_4$) on phase behavior of poly(styrene-*b*-isoprene-*b*-ethylene oxide) (PS-*b*-PI-*b*-PEO) and poly(isoprene-*b*-styrene-*b*-ethylene oxide) (PI-*b*-PS-*b*-PEO) triblock copolymers and found an increase of ODT and microdomain spacing.[15,16] They attributed the changes to the increase in χ and changes in PEO chain statistics. Recently, an increase of the ODT and microdomain spacing were also observed in PS-*b*-P2VP copolymers complexing with cadmium chloride ($CdCl_2$).[17] Rather than arguing the increase in χ, the authors suggested that the changes in conformation of P2VP arising from coordination of P2VP with Cd ions gave rise to the changes in phase behavior. In contrast to these copolymers, PS-*b*-PMMA copolymers have relatively weak interactions between metal ions and carbonyl groups. Even though an increase in χ induced by

* To whom correspondence should be addressed: e-mail russell@mail.pse.umass.edu.
† University of Massachusetts.
‡ Université Catholique de Louvain-La-Neuve.

10.1021/ma071908d CCC: $40.75
Published on Web 01/10/2008

Table 1. Copolymer Characteristics

	M_w (kg/mol)	f_{PS}	PDI	morphology
dPS-*b*-PMMA[a]	28	0.53	1.07	phase-mixed
PS-*b*-PMMA	76	0.94	1.06	phase-mixed
PS-b-PMMA	62	0.53	1.07	lamella
PS-*b*-PMMA	86	0.75	1.07	cylinder
PS-*b*-PMMA	92	0.86	1.06	sphere
dPS-*b*-dPMMA[b]	128	0.88	1.05	sphere

[a] The PS block of the copolymer is labeled with deuterium to provide a contrast for neutron scattering. [b] Both PS and PMMA block are labeled with deuterium. Although the interaction between PS and PMMA may be slightly changed by the deuteration of either block, it is not of significance to the studies presented here.[18]

lithium−PMMA complexes has been proposed, it is not clear how ionic complexes with a weak coordination interaction will affect phase behavior of PS-*b*-PMMA copolymers. In this article, we discuss the influence of ionic complexes on the phase behavior of PS-*b*-PMMA copolymers over a wide range of molecular weights and volume fractions. Disorder-to-order transitions (DOT), order-to-order transitions (OOT), and the increase of the microdomain spacing and degree of ordering were observed in both symmetric and asymmetric PS-*b*-PMMA copolymers, suggesting that the formation of ionic complexes in PMMA blocks increases the overall Flory−Huggins segmental interaction parameter, χ_{eff}, between PS and PMMA with complexes in comparison to that of neat copolymers. Similar effects are found when transition metal ions, like Cu^{2+}, are used with PS-*b*-PMMA copolymers.

Experimental Section

Materials. Shown in Table 1 are the PS-*b*-PMMA copolymers used in this study. All the block copolymers were synthesized by sequential living anionic polymerization. The molecular weights were determined by size exclusion chromatography (SEC), calibrated with PS standards. The volume fraction of PS was determined using ^{1}H NMR spectroscopy (400 MHz). Toluene, tetrahydrofuran (THF), lithium chloride (LiCl), and copper chloride ($CuCl_2$) were used as received.

Sample Preparation. To produce ionic complexes in PS-*b*-PMMA copolymers, two solutions of salts (LiCl or $CuCl_2$) in THF (1 wt %) and PS-*b*-PMMA copolymers in toluene were mixed together at a given ratio and continuous stirred with moderate heating at temperature below 50 °C until most of THF was evaporated and the solutions became clear. The difference between "with" and "without" evaporation of THF can be found in ref 12. The added ratio of inorganic ions to carbonyl group is not a critical number but can be used to control the relative percentage of complexes in the copolymers since the interaction between the inorganic ions with carbonyl group in PMMA is rather weak; not all of ions added into the system can form polymer complexes. Some form complexes, some may exist as free ions, and the others may just precipitate. All the solutions we used here were filtered to remove the salt aggregates before running any experiments. All the samples were measured by FT-IR to ensure the formation of ionic complexes and the percentage of carbonyl groups complexed with inorganic ions was calculated (FT-IR spectra and fitting results are provided in the Supporting Information). It should be noted that ∼27% complexation is the highest percentage that we could achieve so far. Thin films of PS-*b*-PMMA were prepared by spin-coating the mixed solutions onto silicon wafers having a native oxide layer. Samples for small-angle X-ray scattering measurements were prepared by drop-casting the mixed solutions onto Kapton films. All samples were annealed at 170 °C under vacuum for 2 days to reach equilibrium states and then quenched to room temperature.

Small-Angle X-ray Scattering (SAXS). SAXS experiments were performed at Materials Research Science and Engineering Center (MRSEC) at the University of Massachusetts, Amherst. A SAXS instrument, consisting of a three-pinhole collimation system, had an Osmic MaxFlux X-ray (Cu Kα, 0.154 nm) source generated by a copper anode. The size of the beam and beam stop was about 0.5 mm and 2.5 mm in diameter, respectively. The sample-to-detector distance (calibrated using silver behenate) was 1189 mm. SAXS data were collected by a 2-dimensional, multiwire proportional detector. All the measurements were performed at room temperature under vacuum with an exposure time of 30−60 min. All SAXS data presented here are raw data and not corrected for background and empty cell scattering. Typical SAXS data are presented within a q range from 0.11 to 1.2 nm^{-1}, as determined by polystyrene homopolymer (see Supporting Information).

Transmission Electron Microscopy (TEM). To prepare TEM samples, a thin layer of carbon (∼20 nm) was evaporated onto the surface of the samples before embedding into epoxy that was cured at 60 °C overnight. The films were removed from the substrate by dipping into liquid N_2. All samples were microtomed at room temperature with a diamond knife and then transferred onto copper grids. The thin sections were exposed to ruthenium tetraoxide vapor for ∼35 min to enhance the contrast. TEM measurements were performed on a JEOL TEM200CX at an accelerating voltage of 200 kV.

Grazing Incidence Small-Angle X-ray Scattering (GISAXS). GISAXS measurements were performed at beamline X22B at National Synchrotron Light Source at Brookhaven National Laboratory using X-rays with a wavelength of $\lambda = 1.517$ Å with an exposure time of 60 s per frame. Typical GISAXS patterns were taken at an incidence angle of 0.2°, above the critical angles of the copolymer and below the critical angle of the silicon substrate. Consequently, the entire structure of copolymer thin films could be detected.

Neutron Reflectivity (NR). Specular NR measurements were performed at the National Institute of Standards and Technology at the National Center for Neutron Research on the NG-7 reflectometer and advanced neutron diffractometer/reflectometer. The wavelength (λ) of neutrons was 4.768 Å with $\Delta\lambda/\lambda = 0.02$.

Results and Discussion

DOT in Symmetric and Asymmetric PS-*b*-PMMA Copolymers. It has been argued that the formation of lithium−PMMA complexes significantly increases the segmental interaction between the two blocks.[13] If this argument holds, then it should be possible to drive a phase-mixed PS-*b*-PMMA copolymer into the microphase-separated state by ionic complexation. SAXS and TEM results of a neat symmetric dPS-*b*-PMMA copolymer ($M_n = 28$ kg/mol) and the copolymer with lithium−PMMA complexes show evidence of a DOT (Figure 1). SAXS profile for the neat copolymer exhibits a single, broad peak with a maximum at $q_{max} = 0.346$ nm^{-1} and a full width at half-maximum (fwhm) of 0.103 nm^{-1} (Figure 1A), in agreement with previous studies.[10] This may indicate that the neat copolymer is in the phase-mixed state. After ∼17% carbonyl groups are complexed with lithium ions, the reflection sharpens (fwhm of 0.078 nm^{-1}) and shifts to the left at $q_{max} =$ 0.325 nm^{-1} (Figure 1B). With increasing addition of lithium ions and complexation (up to ∼27%), the reflection continues to sharpen (fwhm of 0.054 nm^{-1}) and shift to an even lower q ($q_{max} = 0.320$ nm^{-1}) (Figure 1C). The continuous shift to a smaller q and the sharpening of the reflection suggest that the copolymer may be driven from a phase-mixed into a microphase-separated state; i.e., a DOT occurs.[10,19] TEM images further support the presence of a DOT and demonstrate this transformation more directly. Shown in Figure 1a is a typical image of a phase-mixed block copolymer, in agreement with the SAXS data. For the copolymer with ∼17% complexes, large grains of lamellae appear in a disordered matrix (Figure 1b). At ∼27%, well-developed lamellae with a long period of 19.6 nm are seen.

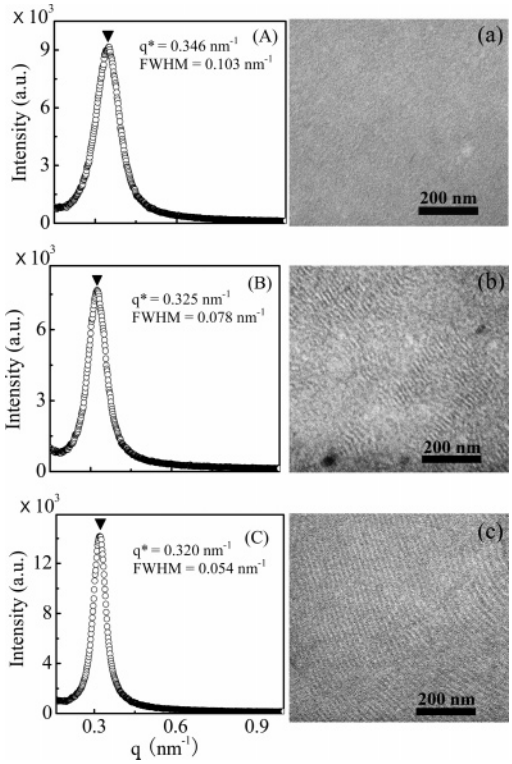

Figure 1. Left: SAXS profiles for the neat symmetric dPS-*b*-PMMA copolymer (M_n = 28 kg/mol) (A) and the copolymer where ~17% (B) and ~27% (C) of carbonyl groups coordinate to lithium ions, after thermal annealing at 170 °C for 2 days followed by quenching to room temperature. Right: corresponding TEM images.

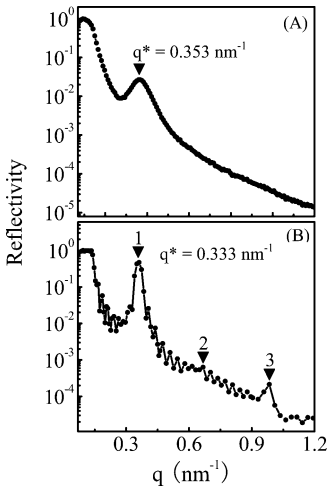

Figure 2. Neutron reflectivity profiles for films of a neat symmetric dPS-*b*-PMMA copolymer (M_n = 28 kg/mol) (A) and the copolymer where ~27% of carbonyl groups coordinate to lithium ions (B) on the native oxide silicon wafers, after thermal annealing at 170 °C for 2 days followed by quenching to room temperature.

The DOT was further examined in films by NR and TEM. Figure 2 shows neutron reflectivity profiles for films of the neat copolymer and the copolymer with ~27% of the carbonyl groups complexed with lithium ions. The NR profile for the neat copolymer film shows a broad reflection near $q^* = 0.353$ nm^{-1} which stems from surface induced ordering[20,21] (Figure 2A). The absence of well-defined Bragg reflections indicates that there is no significant orientation of lamellar microdomains with respect to the surface, in agreement with the TEM observations (Figure 3A). The NR profile for the film containing lithium−PMMA complexes is markedly different (Figure 2B). The presence of a sharp, intense peak at $q^* = 0.333$ nm^{-1},

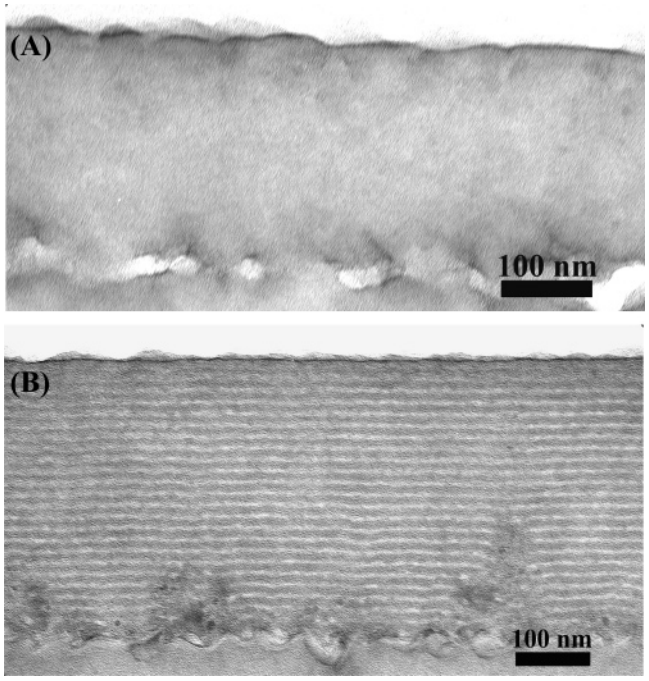

Figure 3. Cross-sectional TEM images of films of a neat symmetric dPS-*b*-PMMA copolymer (M_n = 28 kg/mol) (A) and the copolymer where ~27% of carbonyl groups coordinate to lithium ions (B), after thermal annealing at 170 °C for 2 days followed by quenching to room temperature.

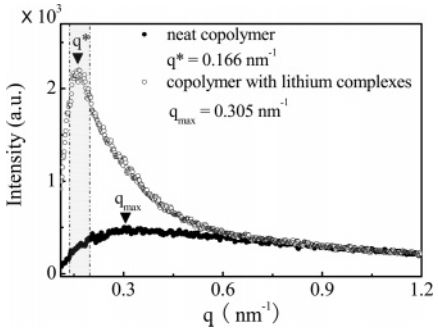

Figure 4. SAXS profiles for a neat PS-*b*-PMMA copolymer (M_n = 76 kg/mol and f_{PS} = 0.94) (●) and the copolymer where ~27% of carbonyl groups coordinate to lithium ions (○), after thermal annealing at 170 °C for 2 days followed by quenching to room temperature.

together with the higher order reflections, indicates that the copolymer film with lithium−PMMA complexes microphase-separates into alternating dPS and PMMA multilayers, consistent with the cross-sectional TEM image (Figure 3B). Consequently, the copolymer has undergone a transition from a phase-mixed to a microphase-separated state with the formation of lithium−PMMA complexes.

The DOT induced by lithium−PMMA complexes was also seen with an asymmetric PS-*b*-PMMA copolymer with a molecular weight of 76 kg/mol and a PS volume fraction of 0.94. The SAXS profile for neat asymmetric copolymer (Figure 4) shows a very broad peak at $q_{max} = 0.305$ nm^{-1}, which is attributed to the correlation hole effect.[6,22,23] With lithium−PMMA complexes, the peak is more pronounced and significantly sharpened especially in the q range of 0.1322−0.2043 nm^{-1} (noted by the dashed line in Figure 4) with q^* at 0.166 nm^{-1}. The peak is broad in the q range of 0.2277−0.3967 nm^{-1}, where the higher orders should be seen, if the spherical domains are ordered on a lattice. The strong decrease in q_{max} and the broad shoulder in the q range from 0.2277 to 0.3967 nm^{-1} suggest that microphase separation has occurred, but the

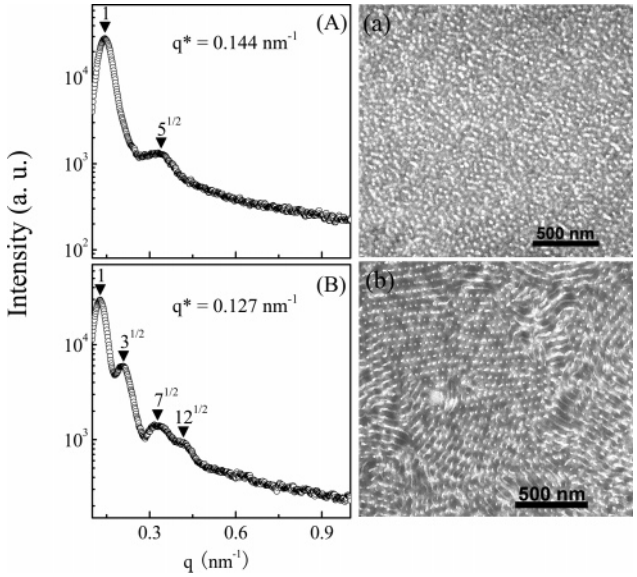

Figure 5. Left: SAXS profiles for a neat dPS-*b*-dPMMA copolymer (M_n = 128 kg/mol and f_{PS} = 0.88) (A) and the copolymer where ~27% of carbonyl groups coordinate to lithium ions (B), after annealing at 170 °C for 2 days followed by quenching to room temperature. Right: corresponding TEM images.

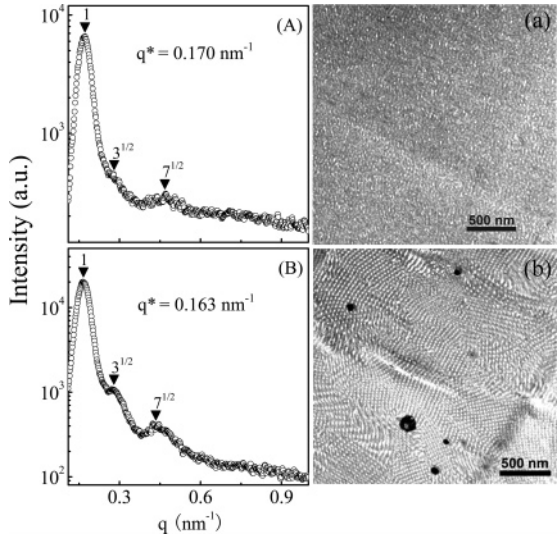

Figure 6. Left: SAXS profiles of a neat PS-*b*-dPMMA copolymer (M_n = 86 kg/mol and f_{PS} = 0.75) (A) and the copolymer where ~17% of carbonyl groups coordinate to lithium ions (B), after thermal annealing at 170 °C for 2 days followed by quenching to room temperature. Right: corresponding TEM images.

spherical microdomains pack in a liquidlike state. Inducing a DOT by lithium−PMMA complexes in both symmetric and asymmetric copolymers further substantiates the conclusion that the overall segmental interaction parameter χ_{eff} is significantly increased by the formation of ionic complexes.

OOT from Spheres to Cylinders. A dPS-*b*-dPMMA copolymer with a molecular weight of 128 kg/mol and dPS volume fraction of 0.88 near the phase boundary between the spherical and cylindrical microdomains was used to examine the possibility of order-to-order transitions. The SAXS profile for the neat copolymer shows two peaks located at $1q^*$ and $5^{1/2}q^*$ (Figure 5A), suggesting a spherical microdomain morphology.[24,25] However, the SAXS profile for the copolymer with lithium−PMMA complexes is distinctly different. The first-order Bragg reflection shifts from 0.144 nm^{-1} for the neat copolymer to 0.127 nm^{-1}, and peaks appear at $1q^*$, $3^{1/2}q^*$, $7^{1/2}q^*$, and $12^{1/2}q^*$, which is characteristic of a hexagonal symmetry (Figure 5B), indicating that the liquidlike packing of spheres changes to either hexagonally packed cylinders or spherical microdomains packed on a hexagonal lattice due to the formation of lithium−PMMA complexes. Real-space observations by TEM were performed to complement the SAXS. The TEM image of the neat copolymer shows only liquidlike packing of spheres (Figure 5a), consistent with the SAXS data. At a high concentration of lithium−PMMA complexes formed in the copolymer (~27% for this case), the hexagonally ordered cylindrical microdomains are seen, demonstrating that an OOT occurs (Figure 5b). The OOT induced by lithium−PMMA complexes can be more clearly seen in the concentration-dependent experiments (see Supporting Information). Thus, all these results confirm the occurrence of an OOT from spheres to cylinders.

Enhanced Ordering and Microdomain Spacing in PS-*b*-PMMA Copolymers. The TEM images show that, above the DOT, the ordering of the lamellar microdomains improves with increasing lithium−PMMA complexes (Figure 1c). What is more, the highly ordered multilayered structure in a copolymer film can persist over ~23 periods (Figure 3B), which has not been observed in thin films of a neat microphase-separated copolymer with a higher molecular weight.[26,27] Similar enhanced ordering was also observed previously in a well-separated symmetric PS-*b*-PMMA copolymer.[13] Besides the enhanced ordering, the increase in the microdomain spacing is another common effect associated with the formation of ionic complexes. This may arise from two possible effects: the stretching of the copolymer chains due to the enhanced segment−segment interaction[14−17,28] or the volume fraction of the additives, such as homopolymers,[29−31] nanoparticles,[32] or small organic molecules.[33,34] To form a high concentration of ionic PMMA complexes, the volume of added salts is calculated to about 0.1−0.3% of the copolymer volume, whereas the microdomain spacing usually increases by ~2 nm, leading to an increase of 4−6% in volume, an order of magnitude higher than the volume of added salts. Therefore, we attribute these striking effects seen in the ordering and spacing of lamellar microdomains mainly to the increase in overall segmental interaction χ_{eff}.

The increased ordering and microdomain spacing were further examined in bulk and thin films of asymmetric copolymers with cylindrical and spherical microdomain morphologies. The SAXS profile for the neat PS-*b*-PMMA copolymer with a molecular weight of 86 kg/mol and a PS volume fraction of 0.75 shows three peaks at $1q^*$, $3^{1/2}q^*$, and $7^{1/2}q^*$ (Figure 6A), indicating a hexagonally packed cylindrical microdomain morphology. PMMA cylinders are distributed in a PS matrix in the corresponding TEM image (Figure 6a), with poor ordering and weak contrast, due to the broad interphase between two microdomains (~5 nm).[35] After lithium−PMMA complexes are formed in the copolymer, the higher ordered reflections at $3^{1/2}q^*$ and $7^{1/2}q^*$ become more intense (Figure 6B), suggesting that the PMMA cylinders packed more orderly, which is in a good agreement with the observation of the higher ordering and better contrast by TEM (Figure 6b). Additionally, the increase in the microdomain spacing is reflected in the decrease in q^* from 0.170 nm^{-1} for the neat copolymer to 0.163 nm^{-1} for the copolymer with lithium−PMMA complexes.

A similar influence of lithium−PMMA complexes on the ordering of the microdomains is also observed in films by GISAXS and TEM. Comparing GISAXS patterns for a neat copolymer film (Figure 7A) and the one containing lithium−PMMA complexes (Figure 7B), a scattering ring, arising from randomly oriented cylinders in the films (marked A), is observed

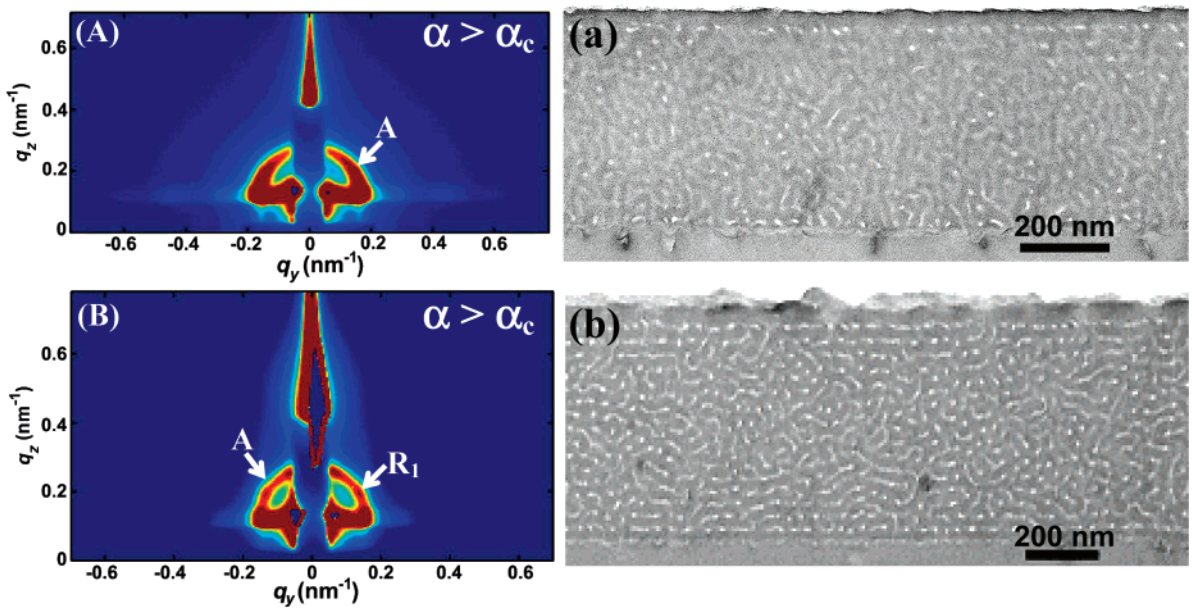

Figure 7. Left: GISAXS patterns of thin films of a neat PS-*b*-dPMMA copolymer (M_n = 86 kg/mol and f_{PS} = 0.75) (A) and the copolymer where ~17% of carbonyl groups coordinate to lithium ions (B), after thermal annealing at 170 °C for 2 days. Right: corresponding TEM images.

in both cases, but the scattering ring from the films with lithium−PMMA complexes is much weaker than that from the neat copolymer films. In addition, two diffraction spots (marked R1) on weakly developed semicircular lines appear in the GISAXS pattern of the film with lithium−PMMA complexes. They are attributed to the first-order Bragg peaks from cylindrical microdomains lying in the film plane, demonstrating a relatively large population of cylinders oriented in that direction.[36] The corresponding TEM images confirm the GISAXS observation in that more cylindrical microdomains oriented in-plane are seen in the films with lithium−PMMA complexes (Figure 7b) than in the neat copolymer (Figure 7a). Thus, an increase in the ordering of cylindrical microdomains is seen with complexation.

The influence of lithium−PMMA complexes on the ordering and spacing is also observed in the asymmetric PS-*b*-PMMA copolymer (M_w = 92 kg/mol and a PS volume fraction of 0.86) that forms a spherical microdomains. The SAXS profile for the neat copolymer shows three peaks at $1q^*$, $2^{1/2}q^*$ (very weak), and $3^{1/2}q^*$ (Figure 8A), indicating a spherical microdomain morphology. Similarly to the case of the cylindrical forming PS-*b*-PMMA copolymer, the SAXS profile for the copolymer with lithium−PMMA (Figure 8B) shows a more distinguishable higher order reflections at $2^{1/2}q^*$ and $3^{1/2}q^*$ with a decrease in q^* from 0.217 nm^{-1} for the neat copolymer to 0.205 nm^{-1}. The corresponding TEM images indicate a significantly enhanced ordering for the copolymer with lithium−PMMA complexes, as evidenced by the highly ordered spherical microdomains packed in a body-centered-cubic (bcc) lattice (Figure 8b). In films, the GISAXS pattern of the neat copolymer film shows several diffraction spots (Figure 9A), which are characteristic of a bcc structure, according to a recent report.[37] These Bragg diffraction spots, however, are elongated and distorted in that position-disordered spheres exist in the bcc lattice, as indicated by the TEM images (Figure 9a). In contrast, the GISAXS pattern of the film with lithium−PMMA complexes (Figure 9B) exhibits much sharper Bragg reflections without any distortion, consistent with the cross-sectional TEM image showing PMMA spherical microdomains are nearly perfectly packed in a bcc lattice (Figure 9b).

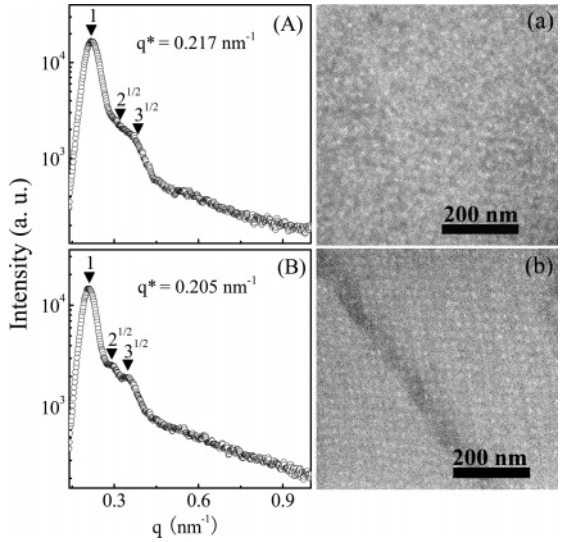

Figure 8. Left: SAXS profiles of a neat PS-*b*-PMMA copolymer (M_n = 92 kg/mol and f_{PS} = 0.86) (A) and the copolymer where ~27% of carbonyl groups coordinate to lithium ions (B), after annealing at 170 °C for 2 days followed by quenching to room temperature. Right: corresponding TEM images.

Influence of Copper−PMMA Complexes. Carbonyl groups in PMMA can interact with different metal ions, such as Cu^{2+}, Ca^{2+}, and Pb^{2+}, to form ionic complexes.[38] Copper−PMMA complexes were formed in a symmetric PS-*b*-PMMA copolymer with a molecular weight of 62 kg/mol to study the influence of different ionic complexes on the phase behavior of PS-*b*-PMMA copolymers. Figure 10 shows SAXS profiles and TEM images of the neat copolymer and the copolymer where ~17% and ~27% of the carbonyl groups have been complexed with copper ions, respectively. The first-order Bragg reflection q^* shifts from 0.181 nm^{-1} for the neat copolymer to 0.176 nm^{-1} for the copolymer with copper−PMMA complexes and the intensity of $2q^*$ and $3q^*$ relative to q^* increases, indicating that the microdomain spacing and degree of ordering are enhanced by the formation of copper−PMMA complexes. The increased

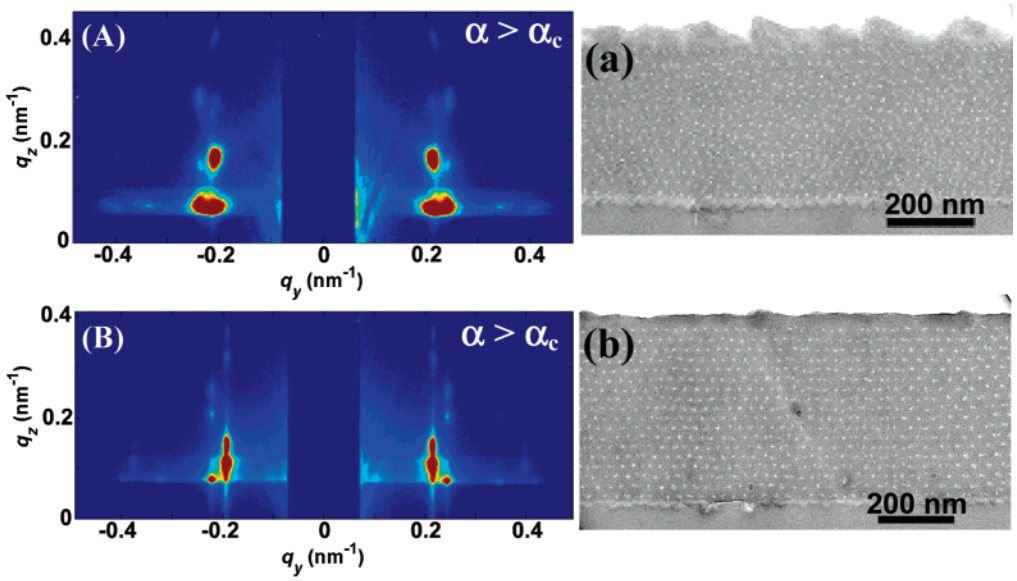

Figure 9. Left: GISAXS patterns of thin films of a neat PS-*b*-PMMA copolymer (M_n = 92 kg/mol and f_{PS} = 0.86) (A) and the copolymer where ~27% of carbonyl groups coordinate to lithium ions (B), after thermal annealing at 170 °C for 2 days. Right: corresponding TEM images.

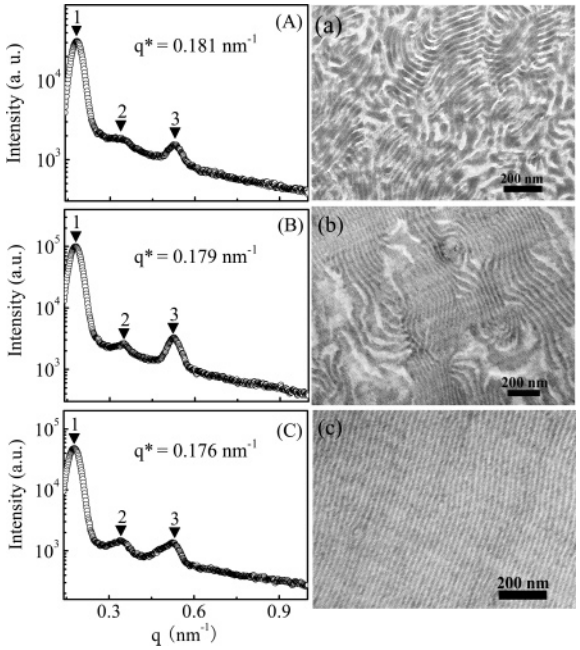

Figure 10. Left: SAXS profiles for a neat PS-*b*-PMMA copolymer (M_n = 62 kg/mol and f_{PS} = 0.53) (A) and the copolymers where ~17% (B) and ~27% (C) of carbonyl groups coordinate to copper ions, after thermal annealing at 170 °C for 2 days followed by quenching to room temperature; Right: corresponding TEM images.

ordering of copolymers observed by TEM is more pronounced. With increasing copper−PMMA complexes, grain sizes become larger and the density of the defects decreases. Up to ~27% of the carbonyl groups complexed with copper ions, grains are so large that few defects can be seen over ~2.5 × 2.5 μm^2 (see Supporting Information). All these effects are similar to that seen with the lithium−PMMA complexes in the symmetric PS-*b*-PMMA copolymer with a molecular weight of 57 kg/mol (reported previously[13]), implying that the copper−PMMA complexes play an identical role as the lithium−PMMA complexes in PS-*b*-PMMA copolymers to enhance the repulsive interaction, χ_{eff}.

Conclusions

We have shown the influence of ionic complexes on phase behavior of PS-*b*-PMMA copolymers in the bulk and thin films. DOT in both symmetric and asymmetric PS-*b*-PMMA copolymers was seen, indicating that the overall segmental interaction χ_{eff} is significantly increased as a result of ionic complex formation. The enhanced χ_{eff} leads to the occurrence an OOT from spheres to cylinders and an increase in ordering and spacing of copolymer microdomains. Concentration-dependent studies demonstrated that χ is highly dependent on the concentration of ionic complexes, providing an additional tool to tune the degree of microphase separation of PS-*b*-PMMA copolymers. Furthermore, the addition of transitional metal ions, which can be reduced to metal particles, makes it possible to incorporate different functionalities into copolymers, offering a way to fabricate luminescent, electric, magnetic, and nonlinear optical materials.

Acknowledgment. This research was supported by the Department of Energy Basic Energy Science (DEFG0296ER45612) and the National Science Foundation-supported Material Research Science and Engineering Center at the University of Massachusetts, Amherst (DMR-0213695). We thank Dr. S. K. Satija and Prof. T. Xu for the assistance with neutron reflectivity measurements and Dr. B. M. Ocko for the assistance with GISAXS experiments. We acknowledge the support of the National Institute of Standards and Technology, U.S. Department of Commerce, in providing the neutron research facilities used in this work. Use of the National Synchrotron Light Source, Brookhaven National Laboratory, was supported by the U.S. Department of Energy, Office of Science, Office of Basic Energy Sciences, under Contract DE-AC02-98CH10886.

Supporting Information Available: Typical FT-IR absorption spectra for PS-*b*-PMMA copolymers with lithium complexes, a scattering profile of polystyrene homopolymer, concentration-dependent OOT experimental results, and a large size TEM image of PS-*b*-PMMA copolymer with ~27% of copper complexes. This material is available free of charge via the Internet at http://pubs.acs.org.

References and Notes

(1) Hawker, C. J.; Russell, T. P. *MRS Bull.* **2005**, *30*, 952.
(2) Bates, F. S.; Fredrickson, G. H. *Phys. Today* **1999**, *52*, 32.
(3) Lodge, T. P. *Macromol. Chem. Phys.* **2003**, *204*, 265.
(4) Segalman, R. A. *Mater. Sci. Eng., R* **2005**, *48*, 191.
(5) Bates, F. S. *Science* **1991**, *251*, 898.
(6) Leibler, L. *Macromolecules* **1980**, *13*, 1602.
(7) Cavicci, K. A.; Russell, T. P. *Macromolecules* **2007**, *40*, 1181.
(8) Ryu, D. Y.; Shin, K.; Drockenmuller, E.; Hawker, C. J.; Russell, T. P. *Science* **2005**, *308*, 236.
(9) Thurn-Albrecht, T.; Schotter, J.; Kästle, G. A.; Emley, N.; Shibauchi, T.; Krusin-Elbaum, L.; Guarini, K.; Black, C. T.; Tuominen, M. T.; Russell, T. P. *Science* **2000**, *290*, 2126.
(10) Russell, T. P., Jr.; Hjelm, R. P.; Seeger, P. A. *Macromolecules* **1990**, *23*, 890.
(11) Xu, T.; Kim, H.-C.; DeRochey, J.; Seney, C.; Levesque, C.; Martin, P.; Stafford, C. M.; Russell, T. P. *Polymer* **2001**, *42*, 9091.
(12) Wang, J. Y.; Xu, T.; Leiston-Belanger, J.; Gupta, S.; Russell, T. P. *Phys. Rev. Lett.* **2006**, *96*, 128301.
(13) Wang, J. Y.; Leiston-Belanger, J. M.; Sievert, J. D.; Russell, T. P. *Macromolecules* **2006**, *39*, 8487.
(14) Ruzette, A. G.; Soo, P. P.; Sadoway, D. R.; Mayes, A. M. *J. Electrochem. Soc.* **2001**, *148*, A537.
(15) Epps, T. H., III; Bailey, T. S.; Pham, H. D.; Bates, F. S. *Chem. Mater.* **2002**, *14*, 1706.
(16) Epps, T. H., III; Bailey, T. S.; Waletzko, R.; Bates, F. S. *Macromolecules* **2003**, *36*, 2873.
(17) Lee, D. H.; Kim, H. Y.; Kim, J. K.; Huh, J.; Ryu, D. Y. *Macromolecules* **2006**, *39*, 2027.
(18) Russell, T. P.; Karis, T. E.; Gallot, Y.; Mayes, A. M. *Nature (London)* **1994**, *368*, 729.
(19) Ryu, D. Y.; Lee, D. H.; Jeong, U.; Yun, S.-H.; Park, S.; Kwon, K.; Sohn, B.-H.; Chang, T.; Kim, J. K. *Macromolecules* **2004**, *37*, 3717.
(20) Fredrichson, G. H. *Macromolecules* **1987**, *20*, 2535.
(21) Anastasiadis, S. H.; Russell, T. P.; Satija, S. K.; Majkrzak, C. F. *Phys. Rev. Lett.* **1989**, *62*, 1852.
(22) Bates, F. S. *Macromolecules* **1987**, *20*, 2221.
(23) Mori, K.; Okawara, A.; Hashimoto, T. *J. Chem. Phys.* **1996**, *104*, 7765.
(24) Sakamoto, N.; Hashimoto, T.; Han, C. D.; Kim, D.; Vaidya, N. Y. *Macromolecules* **1997**, *30*, 1621.
(25) Kimishima, K.; Koga, T.; Hashimoto, T. *Macromolecules* **2000**, *33*, 968.
(26) Menelle, A.; Russell, T. P.; Anastasiadis, S. H.; Satija, S. K.; Majkrzak, C. F. *Phys. Rev. Lett.* **1992**, *68*, 67.
(27) Xu, T.; Hawker, C. J.; Russell, T. P. *Macromolecules* **2003**, *36*, 6178.
(28) Almdal, A.; Rodedale, J. H.; Bates, F. S.; Wignall, G. D.; Fredrickson, G. H. *Phys. Rev. Lett.* **1990**, *65*, 1112.
(29) Tanaka, H.; Hasegawa, H.; Hashimoto, T. *Macromolecules* **1991**, *24*, 240.
(30) Jeong, U.; Kim, H.-C.; Rodriguez, R. L.; Tsai, I. Y.; Stafford, C. M.; Kim, J. K.; Hawker, C. J.; Russell, T. P. *Adv. Mater.* **2002**, *14*, 274.
(31) Ahn, D.; Sancaktar, E. *Adv. Funct. Mater.* **2006**, *16*, 1950.
(32) Haryono, A.; Binder, W. H. *Small*, **2006**, *2*, 600.
(33) Ikkala, O.; Brinke, G. T. *Science* **2002**, *295*, 2407.
(34) Sidorenko, A.; Tokarev, I.; Minko, S.; Stamm, M. *J. Am. Chem. Soc.* **2003**, *125*, 12211.
(35) Anastasiadis, S. H.; Russell, T. P.; Satija, S. K.; Majkrzak, C. F. *J. Chem. Phys.* **1990**, *92*, 5677.
(36) Lee, B.; Park, I.; Yoon, J.; Park, S.; Kim, J.; Kim, K.-W.; Chang, T.; Ree, M. *Macromolecules* **2005**, *38*, 4311.
(37) Stein, G. E.; Kramer, E. J.; Li, X.; Wang, J. *Macromolecules* **2007**, *40*, 2453.
(38) Zhu, J.; Goetsch, P.; Ruzycki, N.; Campbell, C. T. *J. Am. Chem. Soc.* **2007**, *129*, 6432.

MA071908D